LEE, A. VAN DER, BOUWMEESTER, H. & WIEGERS, G. A. (1989). In preparation.
LE PAGE, Y. (1982). *J. Appl. Cryst.* **15**, 255-259.
MAAREN, M. H. VAN (1972). *Phys. Lett.* **40**, 353-354.
MCCANDLISH, L. E., STOUT, G. H. & ANDREWS, L. C. (1975). *Acta Cryst.* A**31**, 245-249.
MAKOVICKY, E. & HYDE, B. G. (1981). *Struct. Bonding (Berlin)*, **46**, 101-170.
MURUGESAN, T., RAMESH, S., GOPALAKRISHNAN, J. & RAO, C. N. R. (1981). *J. Solid State Chem.* **38**, 165-172.
OTERO-DIAZ, L., FITZGERALD, J. D., WILLIAMS, T. B. & HYDE, B. G. (1985). *Acta Cryst.* B**41**, 405-410.
PAULUS, W., MEETSMA, A., BOER, J. L. DE & WIEGERS, G. A. (1989). In preparation.
SCHMIDT, L. (1970). *Phys. Lett.* **31**A, 551-552.
SCHNERING, H. G. VON & WIEDEMEIER, H. (1981). *Z. Kristallogr.* **156**, 143-150.
SHELDRICK, G. M. (1986). *SHELXS*86. Program for crystal structure solution. Univ. of Göttingen, Federal Republic of Germany.
SMAALEN, S. VAN (1989). *J. Phys. C.* Submitted.
SPEK, A. L. (1982). *The EUCLID Package.* In *Computational Crystallography*, edited by D. SAYRE, p. 528. Oxford: Clarendon Press.
SPEK, A. L. (1983). Proc. 8th Eur. Crystallogr. Meet., Belgium.
STERZEL, W. & HORN, J. (1970). *Z. Anorg. Allg. Chem.* **376**, 254-260.
WIEDEMEIER, H. & VON SCHNERING, H. G. (1978). *Z. Kristallogr.* **148**, 295-303.
WIEGERS, G. A., MEETSMA, A., HAANGE, R. & BOER, J. L. DE (1988). *Mater. Res. Bull.* **23**, 1551-1559.

*Acta Cryst.* (1989). A**45**, 291-296

# The Incommensurate Misfit Layer Structure of $(SnS)_{1.17}NbS_2$, '$SnNbS_3$'. II. A Study by Means of Electron Microscopy

BY S. KUYPERS,* G. VAN TENDELOO, J. VAN LANDUYT AND S. AMELINCKX

*University of Antwerp (RUCA), Groenenborgerlaan* 171, *B*-2020 *Antwerpen, Belgium*

(*Received* 12 *July* 1988; *accepted* 25 *October* 1988)

## Abstract

Electron diffraction and high-resolution imaging are used to study the remarkable incommensurable misfit layer compound $(SnS)_{1.17}NbS_2$, '$SnNbS_3$'. Electron diffraction patterns along the zone axis perpendicular to the layer planes are analysed in detail based on the mixed-layer assumption proposed in paper I [Meetsma, Wiegers, Haange & de Boer (1989). *Acta Cryst.* A**45**, 285-291]. The relative intensities of the *hk*0 reflections due to the two types of constituent layers are strongly influenced by the foil thickness. Stacking variants along the *c* axis are frequently observed and strongly complicate the diffraction patterns. Under particular conditions of thickness and defocus, high-resolution images are shown to reflect the varying degree of coincidence of the atom columns in the misfit layers and thus they directly reveal the incommensurate misfit.

## 1. Introduction

In paper I (Meetsma, Wiegers, Haange & de Boer, 1989) the structure determination by means of X-ray diffraction from single crystals of the compound $(SnS)_{1.17}NbS_2$, '$SnNbS_3$', a member of the series $MTX_3$ ($M$ = Sn, Pb; $T$ = Ti, V, Nb, Ta; $X$ = S, Se), was reported. The compound was found to consist of a periodic alternation of SnS layers and $NbS_2$ layers along a common *c* axis (Fig. 3 of paper I). The SnS layers have a slightly deformed NaCl-type structure, whereas the $NbS_2$ layers have the hexagonal (trigonal prismatic) $NbS_2$-2*H* structure. Both structures can be described with reference to *C*-centred orthorhombic unit cells with lattice parameters: $a = 5{\cdot}673$, $b = 5{\cdot}750$, $c = 11{\cdot}760$ Å for SnS and $a' = 3{\cdot}321$, $b' = 5{\cdot}752$, $c' = 11{\cdot}763$ Å for $NbS_2$. The orientation relationship is: $(001)_{SnS} \| (001)_{NbS_2}$; $[010]_{SnS} \| [010]_{NbS_2}$. The unit meshes in the plane of the layers fit along the *b* direction; however, along the *a* direction there is an obvious misfit. The ratio $a/a'$ is approximately 12/7, but in actual fact it may be incommensurate.

Thus far the only electron microscopy study, and in fact also the only structure determination, of a misfit layer compound containing a transition-metal dichalcogenide was reported for $(LaS)_{1.20}CrS_2$, '$LaCrS_3$' (Kato, Kawada & Takahashi, 1977; Otero-Diaz, Fitzgerald, Williams & Hyde, 1985). In the present investigation of $SnNbS_3$, electron diffraction patterns are reported which are very similar to those for $LaCrS_3$ (Otero-Diaz *et al.*, 1985); furthermore, and in contrast with the former study, high-resolution images could be obtained which clearly reveal the incommensurate misfit in the plane of the layers.

* Author to whom correspondence should be addressed.

0108-7673/89/040291-06$03.00 

## 2. Specimen preparation

Owing to the layered nature of the compound under investigation and the weak cohesion between successive layers, thin foils suitable for electron microscopy could easily be obtained by repeated cleavage of the plate-like $SnNbS_3$ single crystals. Obviously a foil obtained in this way will have its foil plane parallel to the layer planes, thus limiting the observations to zones along the normal to these planes, *i.e.* [001] zones. Observations along [*hk*0] zone axes were made at the curled-up edges of (001) foils as well as in specimens obtained by cutting the plate-like crystals (embedded in a resin) perpendicular to the layer planes with an ultramicrotome. Application of the latter technique, however, often resulted in severe structure deformation for this extremely soft material.

## 3. Electron diffraction

### 3.1. *The* [001] *zone pattern*

The simplest and most frequently observed [001] electron diffraction pattern for $SnNbS_3$ is shown in Fig. 1 together with a schematic representation. A similar diffraction pattern was reported earlier by Prodan & Boswell (1980) for a compound with overall composition $Sn_3Nb_2S_6$, obtained in an attempt to grow $Sn_{1/3}NbS_2$ single crystals. However, this pattern was interpreted by these authors as a superposition pattern, due to an epitaxial intergrowth of hexagonal $SnNbS_2$ and monoclinically deformed $SnS_2$. Another interpretation will now be presented, based on the X-ray data of paper I (Meetsma *et al.*, 1989).

In the [001] zone pattern of Fig. 1 a nearly square (*S*) and a hexagonal (*H*) two-dimensional sublattice of intense spots can be distinguished. The square sublattice of spots is due to the slightly deformed NaCl-type structure of the SnS layers, whereas the hexagonal sublattice of spots can be attributed to the hexagonal structure of the trigonal-prismatic $NbS_2$ layers. Along one direction the two sequences of spots coincide. This is in agreement with the perfect fit of the two types of layers along one particular direction, called **b**.

The relative intensities of the diffraction spots due to SnS and $NbS_2$ can vary considerably with foil thickness. Simulated dynamical diffraction patterns show that the relative intensities of the spots due to the $NbS_2$ lattice increase with increasing foil thickness, while the intensities of the spots due to the SnS lattice gradually decrease. Furthermore, it is found that the presence of an extra layer of one type will enhance the intensities of the spots associated with such a type of layer. Similar behaviour can be found qualitatively from kinematical diffraction considerations (§ 3.2) if one assumes a relative shift between successive layers of the same type.

Apart from the intense basic spots, weaker spots are present, the positions of which can be derived from those of the intense spots. Each spot of the hexagonal sublattice is the origin of a square lattice of satellite spots and *vice versa* leading to an intricate pattern of weak spots. Slow cooling of the specimen foil down to liquid-helium temperature does not visibly influence these diffraction spots. These 'satellites' can be understood if one keeps in mind that a beam diffracted by a SnS layer, for instance, can act as an incident beam for the subsequent $NbS_2$ layer and *vice versa*, since the Bragg conditions in thin foils are

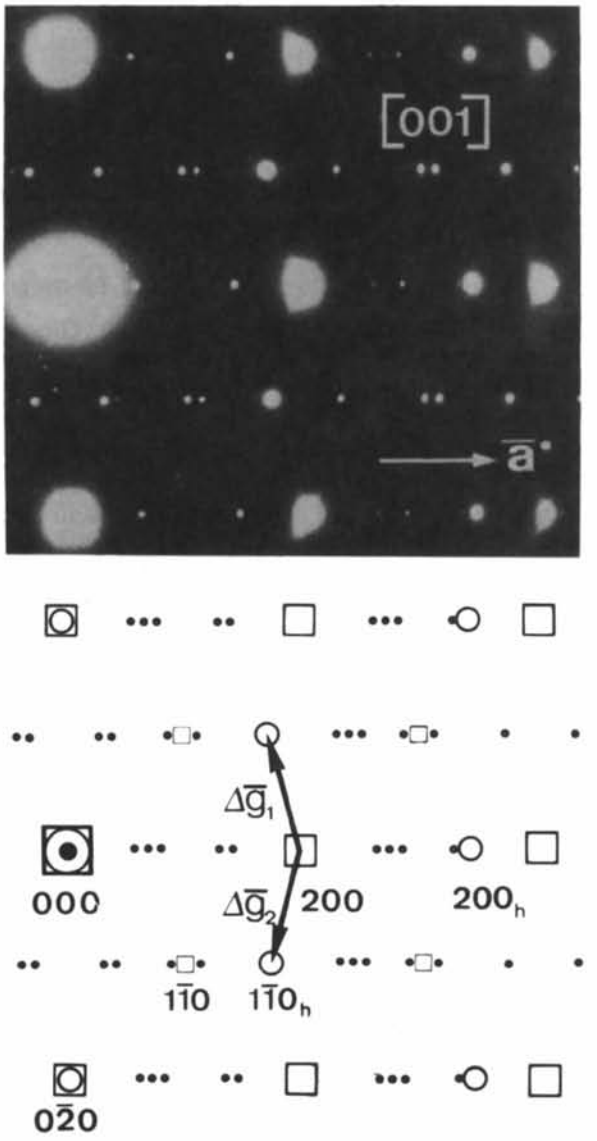


Fig. 1. Electron diffraction pattern along the [001] zone of $SnNbS_3$. The prominent difference vectors $\Delta\mathbf{g}_1$ and $\Delta\mathbf{g}_2$ are indicated. In the schematical representation, the squares, circles and dots correspond to diffraction spots due to the SnS layers, the $NbS_2$ layers and the complete structure, respectively. The indices refer to the orthorhombic unit cells.

considerably relaxed. The diffraction vectors of the compound can thus be written as $\{\mathbf{g}_S\}=\{\mathbf{g}_H\}+\{\mathbf{g}_C\}$, where $\{\mathbf{g}_H\}$ and $\{\mathbf{g}_C\}$ represent the sets of reciprocal-lattice vectors of the hexagonal and the square sublattice of spots respectively. The intensity of a satellite spot will thus be related to the intensity of the basic spots from which it is derived; the former will in general increase with the latter.

The satellite sequences can alternatively be considered as being generated by multiple diffraction, initiated at the basic reflections, by the difference vectors $\Delta\mathbf{g}_1$ and $\Delta\mathbf{g}_2$ between the most intense spots of both sublattices (Fig. 1):

$$\Delta\mathbf{g}_1=\mathbf{g}_{C,1}-\mathbf{g}_{H,1};\quad \Delta\mathbf{g}_2=\mathbf{g}_{C,1}-\mathbf{g}_{H,2}.$$

The diffraction vectors initiated at the spots of the $H$ sublattice are then given by

$$\mathbf{g}_H+p\Delta\mathbf{g}_1+q\Delta\mathbf{g}_2\in\{\mathbf{g}_S\};\quad p,\ q \text{ integers};$$

and similarly for diffraction vectors initiated at the spots of the $C$ sublattice. The two views lead to the same set of diffraction vectors.

One can also interpret the diffraction pattern in terms of the reciprocal modulation of two interpenetrating structures. A measure of this reciprocal modulation is the extent to which the lattice parameters of the pure constituent layers are modified by their mutual influence in the mixed-layer structure. This modulation is small in the present compounds; the deviations from tetragonal and hexagonal symmetry are very small indeed. The lattice potential $V(\mathbf{r})$ of the composite structure can be represented as the sum of the lattice potentials of the $H$ and $C$ lamellae, *i.e.*

$$V(\mathbf{r})=V_H(\mathbf{r})+V_C(\mathbf{r}),$$

where $V_H(\mathbf{r})$ and $V_C(\mathbf{r})$ are periodic with different unit cells. Because of the mutual modulation the potential of the $H$ lamellae is slightly deformed; the deformation pattern has the unit mesh of the $C$ lamellae and *vice versa*. The lattice potential can thus be written explicitly as

$$V(\mathbf{r})=\sum_{\mathbf{g}_H} V_{\mathbf{g}_H}\exp\{2\pi i\,\mathbf{g}_H\cdot[\mathbf{r}+\mathbf{R}_H(\mathbf{r})]\}+\sum_{\mathbf{g}_C} V_{\mathbf{g}_C}\exp\{2\pi i\,\mathbf{g}_C\cdot[\mathbf{r}+\mathbf{R}_C(\mathbf{r})]\},$$

where $\mathbf{R}_H(\mathbf{r})$ is the displacement field of the $H$ lamellae due to the presence of the $C$ lamellae; $\mathbf{R}_C(\mathbf{r})$ has a similar meaning.

Since the mutual interaction is weak we assume that the periodicity in one layer will only be slightly perturbed by the presence of the other layers. We can develop the periodic displacement field $\mathbf{R}_H$, which has the periodicity of the $C$ lamellae, in a Fourier series;

$$\exp[2\pi i\,\mathbf{g}_H\cdot\mathbf{R}_H(\mathbf{r})]=\sum_{\mathbf{g}_C} W_{\mathbf{g}_H,\mathbf{g}_C}\exp(2\pi i\,\mathbf{g}_C\cdot\mathbf{r}),$$

and similarly

$$\exp[2\pi i\mathbf{g}_C\cdot\mathbf{R}_C(\mathbf{r})]=\sum_{\mathbf{g}_H} W_{\mathbf{g}_C,\mathbf{g}_H}\exp(2\pi i\mathbf{g}_H\cdot\mathbf{r}).$$

As a result the total lattice potential can be written as

$$V(\mathbf{r})=\sum_{\mathbf{g}_H}\sum_{\mathbf{g}_C}[V_{\mathbf{g}_H}W_{\mathbf{g}_H,\mathbf{g}_C}+V_{\mathbf{g}_C}W_{\mathbf{g}_C,\mathbf{g}_H}]\times\exp[2\pi i\,(\mathbf{g}_H+\mathbf{g}_C)\cdot\mathbf{r}].$$

The Fourier transform of this expression shows that the diffraction amplitude will have peaks at positions given by the diffraction vectors $\mathbf{h}=\{\mathbf{g}_H\}+\{\mathbf{g}_C\}$, in accordance with our previous conclusions. The amplitude of the peak at $\mathbf{g}_H+\mathbf{g}_C$ depends in a complicated manner on the Fourier coefficients of the reflections $\mathbf{g}_H$ and $\mathbf{g}_C$.

### 3.2. *Kinematical diffraction effects due to a misfit layer structure*

Let us assume that two successive $H$ (or $C$) lamellae in the sequence $HC|HC|\ldots$ are shifted over a vector $\mathbf{R}_s$. This is not unlikely considering the weak cohesive forces between the layers. The component of $\mathbf{R}_s$ parallel to the layer planes is called $\mathbf{R}$; it is not a lattice vector of either $H$ or $C$. We introduce the short notation $\alpha=2\pi\mathbf{g}\cdot\mathbf{R}$, where $\mathbf{g}$ is the active diffraction vector in the type of lamella that is assumed to be diffracting. We exclude common reflections. The structure amplitude can then be written as

$$F_{\mathbf{g}}^{(1)}=F_{\mathbf{g}_H}\sum_{n=0}^{N_1-1}\exp in\alpha,$$

where $N_1$ is the number of $H$ lamellae and $F_{\mathbf{g}_H}$ is the structure amplitude of a single $H$ lamella. We then find the well known result

$$F_{\mathbf{g}}^{(1)}=F_{\mathbf{g}_H}(\sin N_1\alpha/\sin\alpha)\exp[i(N_1-1)\alpha].$$

A similar expression applies to the diffraction by the $C$ lamellae:

$$F_{\mathbf{g}}^{(2)}=F_{\mathbf{G}_C}(\sin N_2\alpha/\sin\alpha)\exp[i(N_2-1)\alpha].$$

If $\mathbf{g}\cdot\mathbf{R}=$ integer then the expressions of course reduce to

$$F_{\mathbf{g}}^{(1)}=N_1F_{\mathbf{g}_H}\quad\text{and}\quad F_{\mathbf{g}}^{(2)}=N_2F_{\mathbf{g}_C},$$

but in general $\mathbf{g}\cdot\mathbf{R}$ will be fractional for both lamellae, say $\mathbf{g}\cdot\mathbf{R}=1/3$. In this case one obtains for $N_1=3$, $F_{\mathbf{g}}^{(1)}=0$; whereas for $N_2=4$ one obtains $F_{\mathbf{g}}^{(2)}=F_{\mathbf{g}_C}$; *i.e.* the intensities of the reflections due to the $C$ lamellae will be larger than those of the reflections due to the $H$ lamellae. Interchanging the number of lamellae, *i.e.* $N_1=4$ and $N_2=3$, changes the relative intensity. According to the kinematic approximation drastic changes in relative intensities of the $\{\mathbf{g}_H\}$ and $\{\mathbf{g}_C\}$ spots can thus occur as a result of a change in thickness by a single lamella. In particular, spots

which are absent if the foil contains an integral number of unit cells ($N_1 = N_2$) can appear if $N_1 = N_2 \pm 1$.

### 3.3. *Other zone patterns*

As already mentioned the layered nature of the compound under investigation strongly limits observations to (001) foils. However, the edge of such a foil seems to have a tendency to curl up around the $b$ axis of the structure, thus permitting observations along the [100] zone axis. An example of a [100] electron diffraction pattern is shown in Fig. 2. The distance between two adjacent spots in a reciprocal row with $k$ = even corresponds with a distance of 11·7 Å in real space, in accordance with the $c$ spacing found from X-ray diffraction. For $k$ = odd, rows of diffuse intensity are often present. They can be associated with relative shifts between successive layers such as presumed in § 3.2.

### 3.4. *Stacking variants*

Owing to the difference in symmetry of the undeformed hexagonal ($H$) and cubic ($C$) lamellae several orientation variants are possible *a priori*. On a $C$ lamella as a substrate, $H$ lamellae can be stacked in two different orientations $H_1$ and $H_2$ differing by 90° (or 30°) in orientation (Fig. 3*a*). Furthermore, each $C$ lamella can be stacked in three orientations, $C_1$, $C_2$, $C_3$, differing 60° in orientation, on a hexagonal lamella as a substrate (Fig. 3*b*). Many stacking sequences are possible and will presumably differ very little in free energy as a result of the quasi-equivalence of the different orientations. One thus not only expects polytypism but also a high degree of stacking disorder.

Complicated stacking sequences or disordered stacking sequences give rise to intricate [001] zone diffraction patterns such as the one shown in Fig. 4. In this pattern only a single orientation variant of the $H$ ($NbS_2$) lamellae is present, but the $C$ (SnS) lamellae occur in three different orientations, $C_1$, $C_2$ and $C_3$. Since the intensities of the different sets of SnS spots are roughly equal, one can assume that the number of SnS lamellae in each of the orientations is nearly equal.

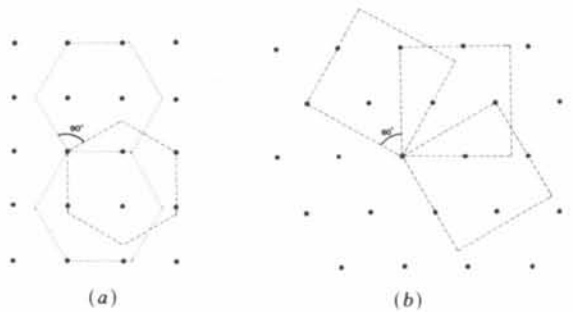


Fig. 3. Schematized view along the [001] zone in $SnNbS_3$ representing: (*a*) the two possible stacking orientations of a hexagonal lamella on a cubic lamella as a substrate; the black dots represent SnS positions; (*b*) the three possible stacking orientations of a cubic lamella on a hexagonal lamella as a substrate; the Nb atoms are represented as black dots.

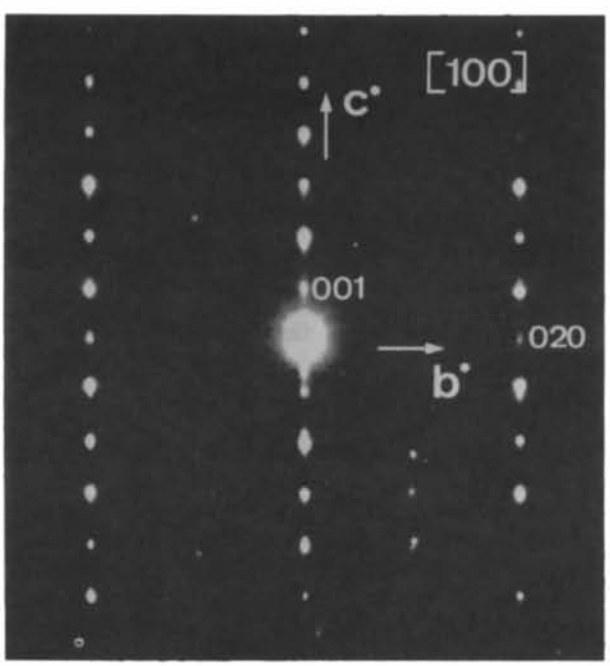


Fig. 2. Electron diffraction pattern along the [100] zone axis of $SnNbS_3$. The rows of diffuse intensity for $k$ = odd are apparent.

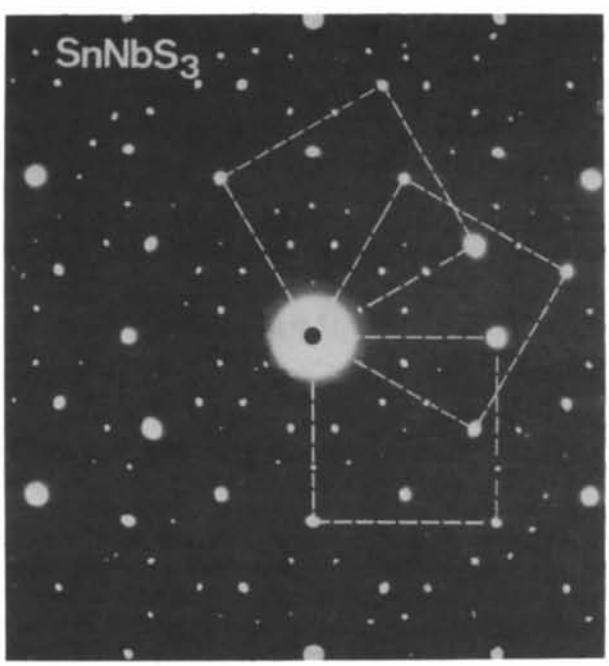


Fig. 4. Intricate diffraction pattern along the [001] zone axis in $SnNbS_3$. The pattern is due to an overlap of a single $NbS_2$ variant and three different SnS variants (outlined).

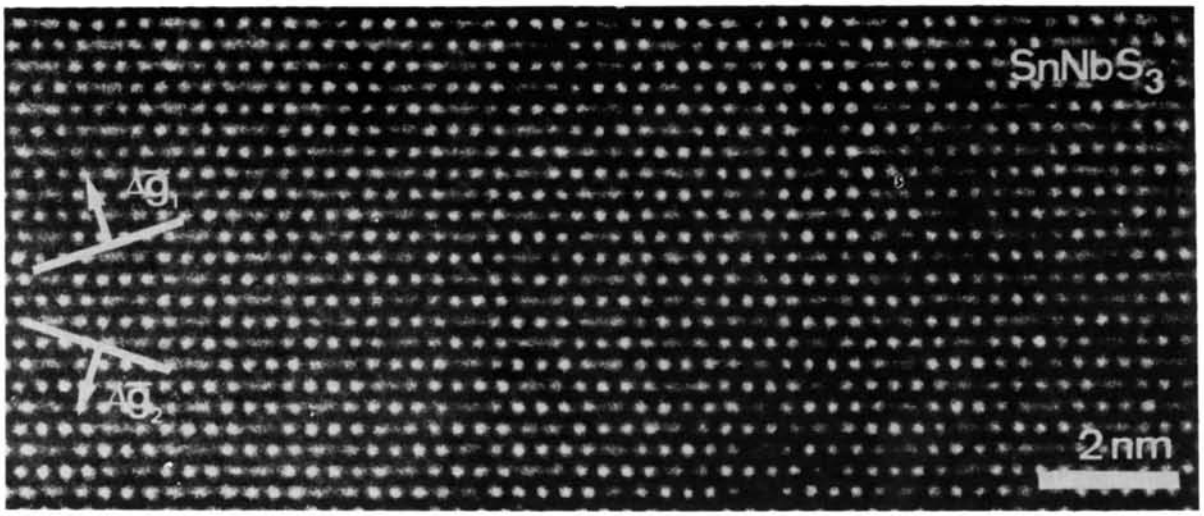


Fig. 5. Example of a high-resolution image as obtained along the [001] zone axis in $SnNbS_3$. The objective aperture radius is 0·5 Å$^{-1}$. The difference vectors $\Delta\mathbf{g}_1$ and $\Delta\mathbf{g}_2$ (Fig. 1) are drawn.

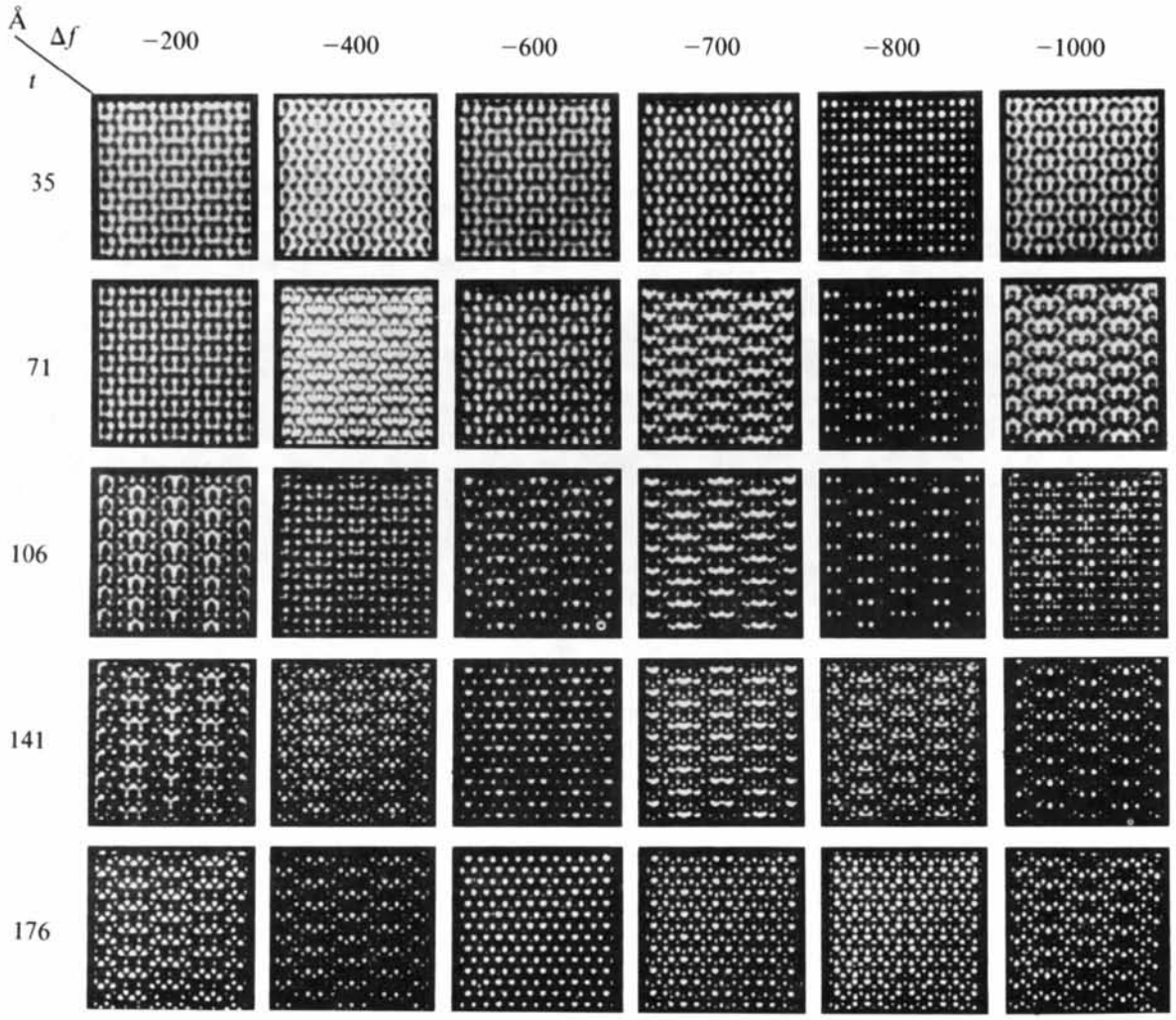


Fig. 6. Matrix of simulated images for $SnNbS_3$ along [001]; $V_a = 200$ kV; $C_s = 1{\cdot}2$ mm; defocus spread: 70 Å; half-angle beam conv.: $8 \times 10^{-4}$ rad; objective aperture radius: 0·5 Å$^{-1}$.

### 4. High-resolution imaging

The most interesting high-resolution images for $SnNbS_3$ were obtained along the [001] zone axis. An example of such an image, corresponding to the diffraction pattern in Fig. 1, is shown in Fig. 5. It consists of arrays of bright dots along the misfit **a** direction. The imaged dots form, depending on focus and thickness of the foil area, a square pattern, a hexagonal pattern or some kind of 'intermediate' pattern. In an intermediate pattern the brightness of the imaged dots varies periodically so as to generate 'intensity waves' with wavevectors $\Delta\mathbf{g}_1$ and $\Delta\mathbf{g}_2$, indicated in Figs. 1 and 5. Such a pattern consists in fact of linear clusters of three or four well defined bright dots separated by diffuse elongated dots; the linear clusters are situated along lines perpendicular to the direction of perfect fit between the layers or, equivalently, along lines perpendicular to the common diffraction vector. The sharp-dot clusters form centred rectangular patterns with a quasi unit cell of the same shape.

Empirically it is known that under certain conditions sharp dots are produced by well defined atom columns. Columns with a composition differing from the normal one will exhibit a different brightness. If the columns are rectilinear but not parallel to the incident electron beam, ill defined and diffuse spots are produced. The effect of column composition was first shown experimentally by means of the superposition pattern of different orientation variants in the ordered alloys $Au_4Mn$ and $Au_5Mn_2$ (Van Tendeloo & Amelinckx, 1978). Image simulations were computed for $Au_4Mn$ (Coene, Van Dyck, Van Tendeloo & Van Landuyt, 1985). The effect of non-rectilinearity of the columns was observed in experimental as well as in simulated images of stacking-fault tetrahedra in silicon (Coene, Bender & Amelinckx, 1985). A small sideways displacement of part of an atom column, as occurs on intersecting a stacking fault, results in a sideways shift of the image dot associated with this column. The magnitude of the shift depends on the level at which the column intersects the stacking fault.

Taking these results into account one can assume that the high-resolution images of the $SnNbS_3$ misfit layer structure will reflect the degree of coincidence of atom columns of the SnS and $NbS_2$ lamellae. To substantiate this assumption a comparison of the experimental images with simulated images for the proposed structure model is required. Image simulations were carried out for $SnNbS_3$. For this purpose an artificial orthorhombic unit cell was used with parameters:

$a = 39{\cdot}78$ Å $(b \sim 7b_C \sim 12b_H)$; $b = 5{\cdot}75$, $c = 11{\cdot}76$ Å.

The accelerating voltage was 200 kV, the spherical aberration constant 1·2 mm, the defocus spread 70 Å and half angle of beam convergence $8 \times 10^{-4}$ rad. The matrix of computed images in Fig. 6 summarizes the results for thicknesses from 35 to 176 Å and for defocus values from −200 to −1000 Å. These simulated images, together with the [001] projection of the structure model (Fig. 4 of paper I), allow us to interpret the experimental images. For the smallest thicknesses and close to Scherzer defocus the simulated images reveal a hexagonal configuration of bright dots for $\Delta f = -600$ Å; whereas for $\Delta f = -800$ Å a square dot configuration is obtained. In the hexagonal situation the positions of the imaged dots correspond to the projected positions of Nb columns in the $NbS_2$ layers. Less-intense diffuse dots appear where Nb columns are (near-) coincident with SnS columns. In the square configuration the dot positions correspond to the positions of SnS columns. Again the less intense dots appear at those sites where the SnS columns are nearly coincident with Nb columns. For large thicknesses, $t > 150$ Å, and near Scherzer defocus, $\Delta f = -600$ Å, the simulated images show hexagonal configurations of bright dots at the projected positions of the Nb columns. At the near-coincidence sites of Nb columns and SnS columns some intensity loss of the dots can still be observed.

The overall behaviour of the simulated images is in good agreement with the experimental images. It can be concluded that, under particular imaging conditions, the experimental images do reflect the pseudo-continuously varying coincidence between the atom columns of the $NbS_2$ layers and those of the SnS layers and in this way they reveal the incommensurate misfit between these layers.

#### References

COENE, W., BENDER, H. & AMELINCKX, S. (1985). *Philos. Mag.* **A52**, 369-381.

COENE, W., VAN DYCK, D., VAN TENDELOO, G. & VAN LANDUYT, J. (1985). *Philos. Mag.* **A52**, 127-143.

KATO, K., KAWADA, I. & TAKAHASHI, T. (1977). *Acta Cryst.* **B33**, 3437-3443.

MEETSMA, A., WIEGERS, G. A., HAANGE, R. J. & DE BOER, J. L. (1989). *Acta Cryst.* **A45**, 285-291.

OTERO-DIAZ, L., FITZGERALD, G. D., WILLIAMS, T. B. & HYDE, B. G. (1985). *Acta Cryst.* **B41**, 405-410.

PRODAN, A. & BOSWELL, F. W. (1980). *Mater. Res. Bull.* **15**, 1763-1766.

VAN TENDELOO, G. & AMELINCKX, S. (1978). *Phys. Status Solidi A*, **47**, 555.